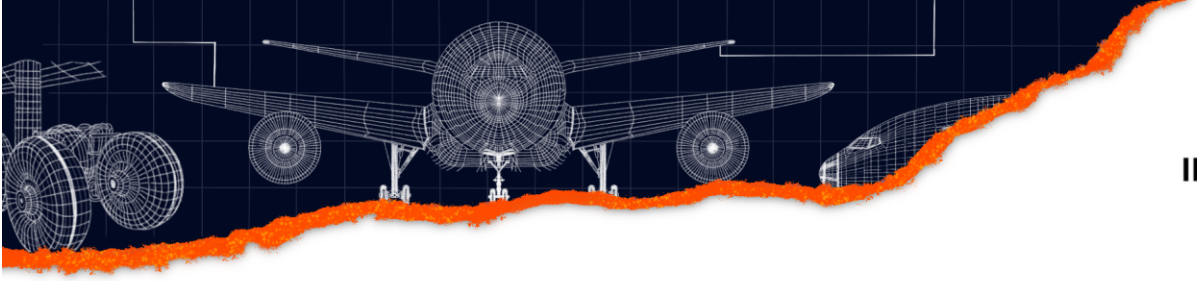

IMPACTO CIENTÍFICO
EDITORA

USE OF THE GENERALIZED INTEGRAL TRANSFORM TECHNIQUE FOR SOLUTION OF THE POPULATION BALANCE EQUATION

USO DA TÉCNICA DE TRANSFORMAÇÃO INTEGRAL GENERALIZADA PARA SOLUÇÃO DA EQUAÇÃO DE EQUILÍBRIO POPULACIONAL

USO DE LA TÉCNICA DE TRANSFORMADA INTEGRAL GENERALIZADA PARA LA SOLUCIÓN DE LA ECUACIÓN DE BALANCE DE POBLACIÓN

https://doi.org/10.56238/edimpacto2025.041-006

Brendo José Wanzeller Moreira[1], Sil Franciley dos Santos Quaresma[2], Clauderino da Silva Batista[3]

ABSTRACT

The population balance equation (PBE), an integro-differential equation, describes the temporal and spatial evolution of particle size distributions in processes such as crystallization, aerosol dynamics, polymerization, and colloidal systems, accounting for phenomena like growth, breakage, aggregation, nucleation, and death. Numerical and hybrid methods have been widely employed to solve the PBE, extending its use across science and engineering. This study applies the generalized integral transform technique (GITT) as a hybrid method to solve the PBE, enabling its transformation into an analytical form and yielding accurate particle size distributions. The method proved efficient and robust, supporting analysis and control in particulate processes.

Keywords: Population Balance Equation. Generalized Integral Transform Technique. Crystallization. Aerosol.

RESUMO

A equação de balanço populacional (EBP), uma equação integro-diferencial, descreve a evolução temporal e espacial das distribuições de tamanho de partículas em processos como cristalização, dinâmica de aerossóis, polimerização e sistemas coloidais, considerando fenômenos como crescimento, quebra, agregação, nucleação e morte. Métodos numéricos e híbridos têm sido amplamente empregados para resolver a EBP, estendendo seu uso à ciência e à engenharia. Este estudo aplica a técnica de transformação integral generalizada (GITT) como um método híbrido para resolver a EBP, permitindo sua transformação em uma forma analítica e produzindo distribuições de tamanho de partículas precisas. O método se mostrou eficiente e robusto, auxiliando na análise e no controle de processos particulados.

[1] Bachelor of Chemical Engineering. Universidade Federal do Pará. E-mail: brendowanzeller@hotmail.com
Orcid: 0009-0005-0252-278X Lattes: https://lattes.cnpq.br/0826133911823854
[2] Doctor in Natural Resources Engineering. Universidade Federal do Pará. E-mail: silquaresma@ufpa.br
Orcid: 0000-0002-1651-7341 Lattes: http://lattes.cnpq.br/6860112313500088
[3] Doctor in Natural Resources Engineering. Universidade Federal do Pará. E-mail: clauderino@ufpa.br
Orcid: 0000-0002-8506-4534 Lattes: https://lattes.cnpq.br/1345689043203622

Palavras-chave: Equação de Balanço Populacional. Técnica de Transformada Integral Generalizada. Cristalização. Aerossol.

RESUMEN

La ecuación de balance de poblaciones (EBP), una ecuación integrodiferencial, describe la evolución temporal y espacial de las distribuciones de tamaño de partícula en procesos como la cristalización, la dinámica de aerosoles, la polimerización y los sistemas coloidales, considerando fenómenos como el crecimiento, la rotura, la agregación, la nucleación y la muerte. Los métodos numéricos e híbridos se han empleado ampliamente para resolver la EBP, extendiendo su uso a la ciencia y la ingeniería. Este estudio aplica la técnica de transformada integral generalizada (GITT) como método híbrido para resolver la EBP, lo que permite su transformación a una forma analítica y proporciona distribuciones de tamaño de partícula precisas. El método demostró ser eficiente y robusto, facilitando el análisis y el control en procesos particulados.

Palabras clave: Ecuación de Equilibrio Poblacional. Técnica de Transformada Integral Generalizada. Cristalización. Aerosol.

1 INTRODUCTION

This study addresses the modeling of particle size distributions in chemical engineering systems via the Population Balance Equation (PBE), an integro-differential formulation that concurrently describes nucleation, growth, aggregation, fragmentation, and particle death phenomena. Given the importance of this tool for processes ranging from crystallization and polymerization to membrane separations and aerosol reactors, various numerical and hybrid solution techniques have been developed to enhance accuracy and computational efficiency. Among these, the Generalized Integral Transform Technique (GITT) stands out by converting the PBE into a system of ordinary differential equations in the transform-coefficient space, enabling an approximate analytical formulation with rapid convergence.

In light of the intrinsic complexity of the PBE and the limitations of purely numerical methods, particularly regarding computational cost and accuracy under non-homogeneous conditions, this work investigates the applicability of GITT to solve the PBE and obtain the particle size density function with high numerical precision. The central research question is whether the GITT-based hybrid methodology yields robust and consistent solutions across different particle process regimes, thereby supporting control and optimization strategies in industrial settings.

This study is justified by the need for analytical tools that combine low computational cost with high reliability in predicting particle population distributions, a critical requirement for the modeling and design of chemical and biochemical processes. By demonstrating GITT's efficacy in resolving the PBE, the research aims to advance more robust mathematical models, directly impacting granulometric property prediction and control development in industrial operations, and deepening scientific understanding of particle population dynamics.

2 THEORETICAL FRAMEWORK

Population Balance Equations (PBE) are extensively used to model particulate systems, such as cell populations, droplets, crystals, polymers, and aerosols, by predicting the evolution of particle property distributions through number balances (Batista, 2011). Initially formulated for Brownian aggregation (Smoluchowski, 1917), PBEs were later extended to include breakage (Rigopoulos; Jones, 2003) and, from the 1960s onward, applied to nucleation and growth, establishing their role in process modeling (Hulburt; Katz, 1964; Randolph, 1969; Drake, 1972; Ramkrishna, 1973, 1985).

Recent developments emphasize numerical and hybrid solution methods, particularly in crystallization (Costa; Maciel; Filho, 2007), as well as reduced-form derivations using group

analysis to simplify systems with aggregation, growth, and nucleation (Pinar, 2021). Applications have also expanded to biological systems, such as viral aggregate size modeling (Zhang; Prigiobbe, 2022). Reviews focused on pharmaceutical crystallization (Lahiq; Alshahrani, 2023) underscore the relevance of the PBE as a versatile and essential tool across scientific and industrial domains. In industrial processes such as solid-liquid separation and drying, particle number and size distributions are critical, with crystallization modeling traditionally relying on the PBE, initially limited to nucleation and growth, and later extended to include aggregation and breakage (Randolph, 1969, 1988; Falope; Jones; Zauner, 2001). The particle size distribution density function is central to the PBE, providing a continuous mass-based description of particle evolution over time. Recent mass-centered reformulations have incorporated all key mechanisms, enhancing the equation's applicability to crystallization and milling processes (Breit; Jakobsen; Von Harbou, 2025).

The strict conservation of mass and increased accuracy in predicting granulometric properties, especially in multimodal and transient distributions, are ensured by the proper use of the population balance equation (Breit; Jakobsen; Von Harbou, 2025). The particle size distribution density function is time-sensitive and influenced by particle interactions, showing higher values for smaller volumes and decreasing as particle volume increases due to aggregation (Batista, 2011). In particulate processes, the particle size distribution (PSD) is a crucial parameter for operational control and product property definition (Alexopoulos; Roussos; Kiparissides, 2024).

Similarly, the crystal size distribution (CSD) and crystal morphology are directly influenced by local concentrations and mixing dynamics, particularly in rapid processes where mixing efficiency governs interparticle interactions (Pagliolico; Marchisio; Barresi, 1999; Jung et al., 2000; Krutzer, 1999; Zauner; Jones, 2000; Sung et al., 2000). In biphasic systems with a continuous phase and a dispersed phase, the latter is represented as a population of particles with coordinated properties. The formulation of the population balance equation for such systems was introduced (Hulburt; Katz, 1964) and consolidated (Ramkrishna, 1985), having been widely employed in the modeling of solid processes and extended to various other scientific fields (Costa, 2007; Pinar, 2021; Zhang, 2022; Lahiq, 2023.

The Population Balance Equation (PBE) describes the temporal evolution of particle number as a function of size in crystallization, accounting for nucleation, growth, aggregation and breakage, while conserving mass and coupling to system mass and energy balances. Numerical solutions employ semi-analytical, sectional or moment methods to capture granulometric changes under varied conditions (Shweta; Hussain; Kumar, 2024). Data-driven

sparse-regression models now infer kinetic kernels directly from limited or noisy time-series, broadening PBE applicability (Tiong; Ahamed; Ho, 2025). Stochastic Monte Carlo techniques further resolve particulate dynamics by modeling random birth–death events, supporting multimodal and transient systems, and complementing deterministic methods (Panicker, 2023).

Crystallization, a cornerstone of the chemical and pharmaceutical sectors, proceeds via spontaneous or heterogeneous nucleation, followed by crystal growth, aggregation and fragmentation, which collectively determine particle size and morphology, and thus purity and downstream performance (Verki et al., 2025). Quantitative description employs the Population Balance Equation (PBE); finite-volume discretization in MSMPR reactors achieves numerical efficiency without sacrificing accuracy in the predicted size-distribution curve (Singh et al. 2020). First-order explicit schemes, e.g. Euler methods augmented with peridynamic operators, maintain computational stability and robustness even amid strong kinetic nonlinearities and fine spatial meshes (Ruan et al., 2024). In continuous operations, such as slug-flow cooling, coupling the PBE with mass and energy balances enables precise control of local supersaturation, resulting in tighter size distributions and enhanced product quality (Kufner, 2023).

Variants of integral transforms, such as those of Melin, Henkel, and Z, have been adapted for specific contexts, proving effective in solving partial differential equations (PDEs), developing numerical methods, and analyzing complex dynamical systems (Debnath; Batha, 2007). Their use has expanded from 19th-century studies to contemporary investigations of nonlinear and chaotic systems, demonstrating both versatility and scientific relevance. In engineering, exact or approximate solutions facilitate interpretation of physical parameters; however, classical methods like separation of variables may be inadequate for PDEs with non-homogeneous boundary conditions. To address such limitations, the Generalized Integral Transform Technique (GITT) was introduced to convert a PDE into an infinite, coupled system of ordinary differential equations, which can be truncated for numerical solution (Ozisik; Murray, 1974).

GITT does not require an exact integral transform, allowing instead the selection of an auxiliary problem with similar characteristics. A transform pair is then constructed using the orthogonality of the auxiliary problem’s eigenfunctions. This generalization extends the method’s applicability to nonlinear problems, surpassing the constraints of classical approaches (Macedo, 1999). By enabling the choice of eigenvalue problems that better reflect the physical system, GITT improves both exact and approximate modeling, even without an explicit transform (Macedo, 1999).

The Generalized Integral Transform Technique (GITT) employs integral transforms to convert partial differential equations, commonly those governing advection–diffusion or conjugate heat and mass transfer, into ordinary differential systems in the transform-coefficient domain, ensuring rapid convergence and high accuracy even with variable coefficients and non-homogeneous boundaries (Cotta; Mikhailov, 1997). By projecting the spatial domain onto orthogonal eigenfunctions, GITT decouples transport and reaction processes, thereby facilitating efficient chemical-engineering simulations with strict conservation (Cotta; Mikhailov, 1997). In contrast to mesh-based schemes for strongly nonlinear, coupled problems, GITT obviates spatial discretization: an analytic transform is applied in all but one coordinate, reducing the numerical effort to solving a single-coordinate ODE system supplemented by algebraic filters derived from simplified governing equations (Miyagawa, 2014). Furthermore, by casting differential operators into algebraic form in the frequency domain, GITT streamlines solution procedures and markedly simplifies the treatment of complex particulate systems via the population balance equation (Dantas; Silva; Oliveira, 2002).

3 METHODOLOGY

In a chemically homogeneous particulate system, the spatial state is described by the size distribution density function $n(v,t)$, where $n(v,t)dv$ represents the number of particles per unit volume within the size range from v to $v+dv$. The system's dynamics, which include growth by adhesion of material from the fluid phase, reduction due to material loss, and coagulation resulting from collisions, are governed by the general particle balance equation (Gelbard; Seinfeld, 1978).

$$\frac{\partial n_v(v,t)}{\partial t} + \frac{\partial [I_v(v,t) n_v(v,t)]}{\partial v} = \int_0^{v/2} \beta_v(v-\tilde{v},\tilde{v}) n_v(v-\tilde{v},t) n_v(\tilde{v},t) d\tilde{v} - n_v(v,t) \int_0^{\infty} \beta_V(v,\tilde{v}) n_v(\tilde{v},t) d\tilde{v} + S_v[n_v(v,t)v,t] \qquad (1)$$

Where: $I_v(v,t) = dv/dt$ expresses the rate of change of particle volume due to material transfer with the fluid phase. The coefficient $\beta_v(v,\tilde{v})$ represents the collision rate between particles of different volumes, and S_v indicates the net rate of new particle formation.

The equation accounts for four terms: individual growth by mass transfer, particle formation through coagulation, particle loss due to collisions, and external sources/sinks. This equation is applied in fields such as colloid chemistry, atmospheric aerosols, crystallization, and population dynamics.

In the proposed methodology, two distinct cases are analyzed, both following the same solution approach. The main difference between Case 1 and Case 2 lies in the second term on the left-hand side of Eq. (1), where the first depends on the spatial variable and the second does not. In both cases, the process begins with a similar initial equation and equivalent boundary conditions, followed by nondimensionalization and the application of necessary algebraic operations to rearrange the equation. This procedure culminates in the application of the GITT.

3.1 CASE I

Case 1 addresses the equation that describes the aerosol phenomenon, demonstrating the behavior of the particle population, represented by Eq. (2.a). Note that in this equation the volume term is within the second differential term, a factor that ends up consistently influencing the behavior of the system.

$$\frac{\partial n(v,t)}{\partial t} + G_0 \frac{\partial [vn(v,t)]}{\partial v} = D_{ab} \frac{\partial^2 n(v,t)}{\partial v^2} + \frac{\beta_0}{2} \int_0^v n(v-\tilde{v},t) n(\tilde{v},t) d\tilde{v} - \beta_0 n(v,t) \int_0^\infty n(\tilde{v},t) d\tilde{v} \qquad (2.a)$$

With these initial and boundary conditions for Eq (2.a):

$$n(v,0) = \frac{N_0}{v_0} e^{\frac{-v}{v_0}}; n(0,t) = 0;\ D_{ab} \frac{\partial n(v,t)}{\partial v} + Gn(v,t) = 0 \qquad (2.b)$$

Which has the following dimensionless groups:

$$\eta = \frac{v}{V};\ \tilde{n}(\eta,\tau) = \frac{n(v,t)V}{N_0};\ \tilde{n}(\eta-\tilde{\eta},\tau) = \frac{n(v-\tilde{v},\tau)V}{N_0};\ \tilde{\eta} = \frac{\tilde{v}}{V};\ \tilde{n}(\tilde{\eta},\tau) = \frac{n(\tilde{v},t)V}{N_0};\ \tau = G_0 t;\ B_{im} = \frac{GVN_0}{D_{ab}} \qquad (3.a\text{-}g)$$

Substituting dimensionless groups into Eq. (2.a) and rearranging the equation, we have:

$$\frac{\partial \tilde{n}(\eta,\tau)}{\partial \tau} + \tilde{n}(\eta,\tau) + \eta \frac{\partial \tilde{n}(\eta,\tau)}{\partial \eta} = \frac{D_{ab}}{G_0 V^2} \frac{\partial^2 \tilde{n}(\eta,\tau)}{\partial \eta^2} + \frac{\beta_0 N_0}{2G_0} \int_0^\eta \tilde{n}(\eta-\tilde{\eta},\tau) \tilde{n}(\tilde{\eta},\tau) d\tilde{\eta} - \frac{\beta_0}{G_0} \tilde{n}(\eta,\tau) \int_0^\infty n(\tilde{v},t) d\tilde{v} \qquad (4)$$

Solving the integral of the last term on the right, we obtain:

$$\int_0^\infty n(\tilde{v},t) d\tilde{v} = M_0 = \frac{2N_0}{2+\beta_0 N_0 t} = \frac{2N_0}{2+(\beta_0 N_0 \tau / G_0)} \qquad (5)$$

Substituting Eq. (5) into Eq. (4) and rearranging the terms algebraically, we obtain:

$$\frac{\partial \tilde{n}(\eta,\tau)}{\partial \tau} + \tilde{n}(\eta,\tau) + \eta \frac{\partial \tilde{n}(\eta,\tau)}{\partial \eta} = A \frac{\partial^2 \tilde{n}(\eta,\tau)}{\partial \eta^2} + B \int_0^{\eta} \tilde{n}(\eta-\tilde{\eta},\tau)\tilde{n}(\tilde{\eta},\tau)d\tilde{\eta} - C\tilde{n}(\eta,\tau) \qquad (6.a)$$

Where each constant is given below:

$$A = \frac{D_{ab}}{G_0 V^2}; \quad B = \frac{\beta_0 N_0}{2G_0}; \quad C = \frac{2\beta_0 N_0}{G_0[2+(\beta_0 N_0 \tau/G_0)]} \qquad (6.b\text{-}d)$$

After dimensioning the differential terms, GITT is applied to Eq. (6.a) in order to remove the independent variable v, where Eq. (7.a) is the integral transform and Eq. (7.b) is its inverse transform (Cotta; Mikhailov, 1997).

$$\bar{n}(\lambda_i,\tau) = \int_0^1 X(\lambda_i,\eta)\tilde{n}(\eta,\tau)d\eta\,; \; \tilde{n}(\eta,\tau) = \sum_{j=1}^{\infty} \frac{X(\lambda_j,\eta)\bar{n}(\lambda_j,\tau)}{N(\lambda_j)} \qquad (7.a,b)$$

Multiplying Equation (6.a) by $X(\lambda_j,\eta)$ and integrating over the interval 0 to 1 in dη, we have:

$$\int_0^1 X(\lambda_i,\eta)\left[\frac{\partial \tilde{n}(\eta,\tau)}{\partial \tau} + \tilde{n}(\eta,\tau) + \eta \frac{\partial \tilde{n}(\eta,\tau)}{\partial \eta} = A \frac{\partial^2 \tilde{n}(\eta,\tau)}{\partial \eta^2} + B \int_0^{\eta} \tilde{n}(\eta-\tilde{\eta},\tau)\tilde{n}(\tilde{\eta},\tau)d\tilde{\eta} - C\tilde{n}(\eta,\tau)\right] d\eta \qquad (8)$$

Solving and rewriting Eq. (8), we obtain:

$$\frac{\partial \bar{n}(\lambda_i,\tau)}{\partial \tau} + \bar{n}(\lambda_i,\tau) + \int_0^1 X(\lambda_i,\eta)\eta \frac{\partial \tilde{n}(\eta,\tau)}{\partial \eta} d\eta = A \int_0^1 X(\lambda_i,\eta) \frac{\partial^2 \tilde{n}(\eta,\tau)}{\partial \eta^2} d\eta + B \int_0^1 X(\lambda_i,\eta)\left[\int_0^{\eta} \tilde{n}(\eta-\tilde{\eta},\tau)\tilde{n}(\tilde{\eta},\tau)d\tilde{\eta}\right]d\eta - C\bar{n}(\lambda_i,\tau) \qquad (9)$$

Applying Green's Theorem (Ozisik; Murray, 1974) to the second-order integro-differential term in Eq. (9), we obtain:

$$\int_0^1 X(\lambda_i,\eta) \frac{\partial^2 \tilde{n}(\eta,\tau)}{\partial \eta^2} d\eta = -\lambda_m^2 \bar{n}(\lambda_i,\tau) \quad (10)$$

Applying Eq. (10) to Eq. (9), we obtain:

$$\frac{\partial \bar{n}(\lambda_i,\tau)}{\partial \tau} + \bar{n}(\lambda_i,\tau) + \int_0^1 X(\lambda_i,\eta)\eta \frac{\partial \tilde{n}(\eta,\tau)}{\partial \eta} d\eta = -A\lambda_m^2 \bar{n}(\lambda_i,\tau) + B \int_0^1 X(\lambda_i,\eta)\left[\int_0^{\eta} \tilde{n}(\eta-\tilde{\eta},\tau)\tilde{n}(\tilde{\eta},\tau)d\tilde{\eta}\right]d\eta - C\bar{n}(\lambda_i,\tau) \qquad (11)$$

Applying the inverse transform in Eq. (11), we obtain:

$$\frac{\partial \bar{n}(\lambda_i,\tau)}{\partial \tau} = -\bar{n}(\lambda_i,\tau) - \sum_{j=1}^{\infty} \bar{n}(\lambda_j,\tau) \int_0^1 \eta \frac{X(\lambda_i,\eta)X^{(\lambda_i,\eta)}}{N(\lambda_j)} d\eta - A\lambda_m^2 \bar{n}(\lambda_i,\tau) + B \int_0^1 X(\lambda_i,\eta)\left[\int_0^{\eta} \sum_{j=1}^{\infty} \frac{\bar{n}(\lambda_j,\tau)X(\lambda_j,\eta)}{N(\lambda_j)} \sum_{k=1}^{\infty} \frac{\bar{n}(\lambda_k,\tau)X(\lambda_k,\eta)}{N(\lambda_k)} d\tilde{\eta}\right] d\eta - C\bar{n}(\lambda_i,\tau) \qquad (12)$$

Rearranging Eq. (12) and applying simplifications, we obtain:

$$\frac{\partial \bar{n}(\lambda_i,\tau)}{\partial \tau} = -[1 + A\lambda_m^2 + c]\bar{n}(\lambda_i,\tau) - \sum_{j=1}^{\infty} \bar{n}(\lambda_j,\tau) \int_0^1 \eta \frac{X(\lambda_i,\eta)X'(\lambda_i,\eta)}{N(\lambda_j)} d\eta + B \sum_{j=1}^{\infty} \sum_{k=1}^{\infty} \frac{\bar{n}(\lambda_k,\tau)\bar{n}(\lambda_j,\tau)}{N(\lambda_j)N(\lambda_k)} \int_0^1 X(\lambda_i,\eta)X(\lambda_j,\eta)X(\lambda_k,\eta)d\eta \quad (13.a)$$

Which has the following initial condition:

$$\bar{n}(\eta,0) = \frac{V}{v_0} \int_0^1 X(\lambda_i,\eta) e^{\frac{-\eta V}{v_0}} d\eta \qquad (13.b)$$

2.2 Case II

Case 2 addresses the phenomenon of crystallization, representing the system's behavior through Eq. (14.a) and the boundary conditions presented in Eq. (14.b-d). It is noteworthy that in this equation, the second differential term does not involve the volume and depends solely on n. This case follows the same methodology applied to the previous case.

$$\frac{\partial n(v,t)}{\partial t} + G\frac{\partial n(v,t)}{\partial v} = D_{ab}\frac{\partial^2 n(v,t)}{\partial v^2} + \frac{\beta_0}{2}\int_0^v n(v-\tilde{v},t)n(\tilde{v},t)d\tilde{v} - \beta_0 n(v,t)\int_0^{\infty} n(\tilde{v},t)d\tilde{v} \qquad (14.a)$$

$$n(v,o) = \frac{N_0}{v_0} e^{\frac{-v}{v_0}} \; ; \; n(0,t) = 0 \; ; \; D_{ab}\frac{\partial n(v,t)}{\partial v} + Gn(v,t) = 0 \qquad (14.b\text{-}d)$$

Which has the following dimensionless groups:

$$\eta = \frac{v}{V} \; ; \; \tilde{n}(\eta,\tau) = \frac{n(v,t)V}{N_0} \; ; \; \tilde{n}(\eta-\tilde{\eta},\tau) = \frac{n(v-\tilde{v},\tau)V}{N_0} \; ; \; \tilde{\eta} = \frac{\tilde{v}}{V} \; ; \; \tilde{n}(\tilde{\eta},\tau) = \frac{n(\tilde{v},t)V}{N_0} \; ; \; \tau = \frac{Gt}{v_0} \; ; \; B_{im} = \frac{GV}{D_{ab}} \qquad (15.a\text{-}g)$$

Substituting dimensionless groups into Eq. (14.a) and rearranging the equation, we have:

$$\frac{\partial \tilde{n}(\eta,\tau)}{\partial \tau} + \frac{v_0}{V}\frac{\partial \tilde{n}(\eta,\tau)}{\partial \eta} = \frac{D_{ab}v_0}{GV^2}\frac{\partial^2 \tilde{n}(\eta,\tau)}{\partial \eta^2} + \frac{\beta_0 N_0 v_0}{2G}\int_0^{\eta} \tilde{n}(\eta-\tilde{\eta},\tau)\tilde{n}(\tilde{\eta},\tau)d\eta - \frac{\beta_0 v_0}{G}\tilde{n}(\eta,\tau)\int_0^{\infty} n(\tilde{v},t)d\tilde{v} \quad (16)$$

Solving the integral of the last term on the right, we obtain:

$$\int_0^{\infty} n(\tilde{v},t)d\tilde{v} = \frac{2N_0}{2+(\beta_0 N_0 \tau v_0/G)} \qquad (17)$$

Substituting Eq. (17) into Eq. (16) and rearranging the terms algebraically, we obtain:

$$\frac{\partial \tilde{n}(\eta,\tau)}{\partial \tau} + A\frac{\partial \tilde{n}(\eta,\tau)}{\partial \eta} = B\frac{\partial^2 \tilde{n}(\eta,\tau)}{\partial \eta^2} + C\int_0^{\eta} \tilde{n}(\eta-\tilde{\eta},\tau)\tilde{n}(\tilde{\eta},\tau)d\tilde{\eta} - D\tilde{n}(\eta,\tau) \qquad (18.a)$$

Where each constant is given below:

$$A = \frac{v_0}{V}; \quad B = \frac{D_{ab} v_0}{GV^2}; \quad C = \frac{\beta_0 N_0 v_0}{2G}; \quad D = \frac{2\beta_0 N_0 v_0}{2G + (\beta_0 N_0 \tau v_0)} \qquad (18.b\text{-}e)$$

After dimensioning the differential terms, GITT is applied in Eq. (18.a) in the same way as in Case 1, using Eq. (7.a) and Eq. (7.b) in order to remove the independent variable v. Multiplying Equation (18.a) by $X(\lambda_j, \eta)$ and integrating over the interval from 0 to 1 in dη, we have:

$$\int_0^1 X(\lambda_i, \eta) \left[\frac{\partial \tilde{n}(\eta,\tau)}{\partial \tau} + A \frac{\partial \tilde{n}(\eta,\tau)}{\partial \eta} = B \frac{\partial^2 \tilde{n}(\eta,\tau)}{\partial \eta^2} + C \int_0^\eta \tilde{n}(\eta - \tilde{\eta}, \tau) \tilde{n}(\tilde{\eta}, \tau) d\tilde{\eta} - D\tilde{n}(\eta, \tau) \right] d\eta \quad (19)$$

Solving and rewriting Eq. (19), we obtain:

$$\frac{\partial \bar{n}(\lambda_i,\tau)}{\partial \tau} + A \int_0^1 X(\lambda_i, \eta) \frac{\partial \tilde{n}(\eta,\tau)}{\partial \eta} d\eta = B \int_0^1 X(\lambda_i, \eta) \frac{\partial^2 \tilde{n}(\eta,\tau)}{\partial \eta^2} d\eta + C \int_0^1 X(\lambda_i, \eta) \left[\int_0^\eta \tilde{n}(\eta - \tilde{\eta}, \tau) \tilde{n}(\tilde{\eta}, \tau) d\tilde{\eta} \right] d\eta - D\bar{n}(\lambda_i, \tau) \qquad (20)$$

Applying Green's Theorem (Ozisik; Murray, 1974) to the second-order integro-differential term in Eq. (20), we obtain the same result found in Eq. (10). Applying Eq. (10) to Eq. (20), we obtain:

$$\frac{\partial \bar{n}(\lambda_i,\tau)}{\partial \tau} + A \int_0^1 X(\lambda_i, \eta) \frac{\partial \tilde{n}(\eta,\tau)}{\partial \eta} d\eta = -B\lambda_m^2 \bar{n}(\lambda_i, \tau) + C \int_0^1 X(\lambda_i, \eta) \left[\int_0^\eta \tilde{n}(\eta - \tilde{\eta}, \tau) \tilde{n}(\tilde{\eta}, \tau) d\tilde{\eta} \right] d\eta - D\bar{n}(\lambda_i, \tau) \qquad (21)$$

Applying the inverse transform in Eq. (21), we obtain:

$$\frac{\partial \bar{n}(\lambda_i,\tau)}{\partial \tau} = -A \sum_{j=1}^{\infty} \bar{n}(\lambda_j, \tau) \int_0^1 \frac{X(\lambda_i,\eta) X'^{(\lambda_i,\eta)}}{N(\lambda_j)} d\eta - B\lambda_m^2 \bar{n}(\lambda_i, \tau) + C \int_0^1 X(\lambda_i, \eta) \left[\int_0^\eta \sum_{j=1}^{\infty} \frac{\bar{n}(\lambda_j,\tau) X(\lambda_j,\eta)}{N(\lambda_j)} \sum_{k=1}^{\infty} \frac{\bar{n}(\lambda_k,\tau) X(\lambda_k,\eta)}{N(\lambda_k)} d\tilde{\eta} \right] d\eta - D\bar{n}(\lambda_i, \tau) 0 \quad (22)$$

Rearranging Eq. (22) and applying simplifications, we obtain:

$$\frac{\partial \bar{n}(\lambda_i,\tau)}{\partial \tau} = -A \sum_{j=1}^{\infty} \bar{n}(\lambda_j, \tau) \int_0^1 \frac{X(\lambda_i,\eta) X'^{(\lambda_i,\eta)}}{N(\lambda_j)} d\eta - B\lambda_m^2 \bar{n}(\lambda_i, \tau) + C \sum_{j=1}^{\infty} \sum_{k=1}^{\infty} \frac{\bar{n}(\lambda_k,\tau) \bar{n}(\lambda_j,\tau)}{N(\lambda_j) N(\lambda_k)} \int_0^1 X(\lambda_i, \eta) X(\lambda_j, \eta) X(\lambda_k, \eta) d\eta - D\bar{n}(\lambda_i, \tau) \qquad (23.a)$$

Which has the following initial condition:

$$\bar{n}(\eta, 0) = \frac{V}{v_0} \int_0^1 X(\lambda_i, \eta) e^{\frac{-\eta V}{v_0}} d\eta \qquad (23.b)$$

3.2 COMPUTATIONAL MODELING

After applying GITT and other techniques to solve the equations, we obtained the analytical solutions for Case 1 and Case 2, as shown in Eq. (13.a,b) and Eq. (23.a,b),

respectively. We proceeded to develop computer codes in Fortran 90/95 language, which were executed in the Process Simulation Laboratory of FEQ/ITEC/UFPA. For the solution, we used the DIVIPAG routine from the IMSLMD library, a widely used routine appropriate for problems such as the one studied in this work. To generate the graphs, we used the Grapher 9 software.

To analyze the behavior of the variables of interest, all others were kept constant. Table 1 contains the values used in the following cases. It should be noted that the process time, crystal size and initial particle number vary from case to case.

Table 1

Terms used in the following cases

Term	Value
Final Time (tf)	Variable
Cristal size (EL)	variable
G	1x10^-1
Beta	1x10^-9
Dab	4x10^-1
Initial particle number (N0)	Variable
Volume initial (V0)	0.015xEL

Source: Authors, 2025.

4 RESULTS AND DISCUSSIONS

After developing the computer codes and processing the data to generate the graphs, solid and quite conclusive results were obtained. To discover their true capacity, several simulations were performed with a wide range of values for the initial number of particles (n_0), time in hours, and volume in cubic meters. For the following graphs, a common value for time and volume was adopted for all, in order to verify the influence of the variation in the initial number of particles in the system. Below are the graphs for both cases for each n_0 and the corresponding conclusions that each one presented.

Figure 1

Graph for a $n_0 = 1x10\text{^}3$

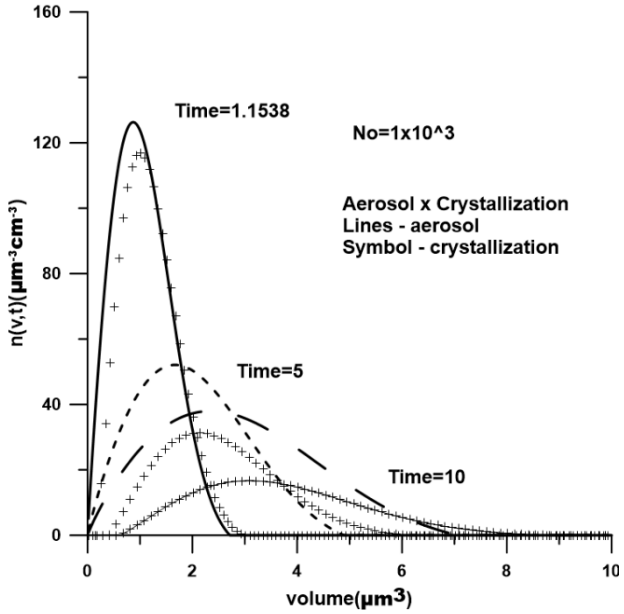

Source: Authors, 2025.

It can be seen that in Fig. 1 the volume density decreases over time, while the volume of the particles increases, a factor that is in agreement with the literature and is justified by the occurrence of collisions between particles that produce larger particles. Another clear piece of information is the relationship between the aerosol and crystallization, where the former reaches lower density values in relation to the latter. This behavior is due to the nature of each process and the tendency of aerosols to dissipate quickly in the medium.

By increasing the process time in the simulations, it can be seen that the graph continues to have the same behavior, with a reduction in density and, consequently, an increase in the volume of the particles. However, due to the low number of particles in the system, they are unable to reach higher values of density and volume due to the lack of matter in the medium, showing that the use of excessively large values of time and volume is irrelevant.

Figure 2

Graph for a $n_0 = 1x10\text{^}5$

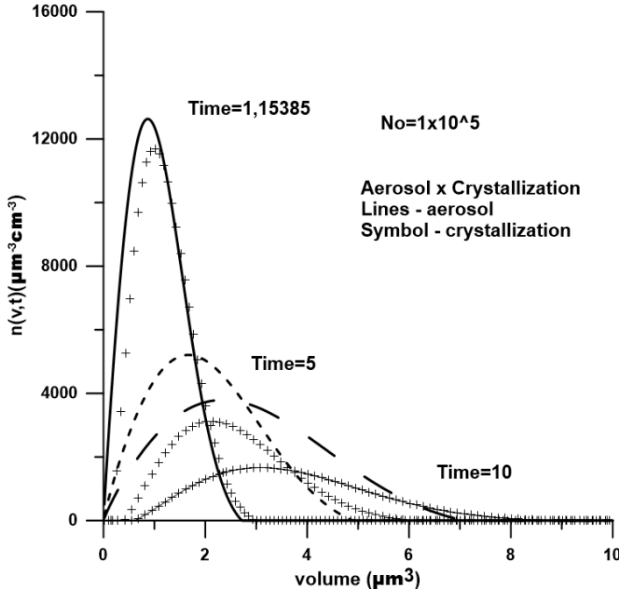

Source: Authors, 2025.

When observing Fig. 2, it is clear that increasing n_0 logically impacts the values obtained, since a high number of particles increases the number of collisions and interactions between them, also encouraging an increase in the population density scale. Furthermore, the graph follows the same behavior as the previous one, where the population density is inversely proportional to time, and the latter, directly proportional to the volume of the particles.

When increasing the simulation time, the graph continues to have a similar curve, maintaining the tendency of reducing particle density while their volume increases. The comparison between aerosols and crystallization remains very clear, with a peak for the aerosol at time 1.15385, which undergoes a considerable reduction at time 5, a reduction that attenuates at time 10 of the simulation. This behavior reinforces the nature of this process. Due to the increase in the number of particles, this system allows a greater variation in time and volume values.

Figure 3

Graph for a $n_0 = 1x10\text{^}7$

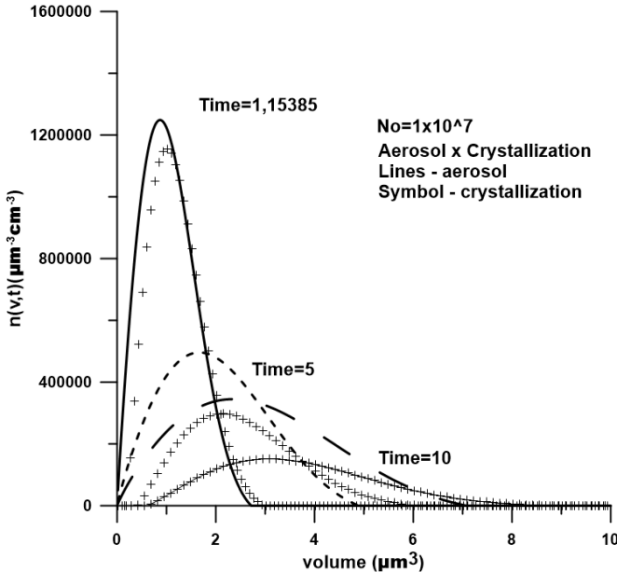

Source: Authors, 2025.

Following the pattern of the previous graphs, Fig. 3 illustrates the behavior for a system with a high number of particles, a factor that influences the magnitude of the population density and volume values, since a greater number of available matter provides a stimulus for an increase in population density, as well as volume. Otherwise, the curves behave similarly to the previous ones, demonstrating solidity and good agreement of the code and model used, in addition to highlighting the difference in the nature of the processes studied, where again, lower values of aerosol population density are observed for each test period.

Due to the increase in initial particles, the scope of time and volume relevant for analysis becomes larger, allowing research and analysis of more complex and broad systems. In order to verify the influence of the variation in time and particle size on the behavior of the system, other simulations were performed keeping the value of n_0 constant, increasing the values of time and particle size. Fig. 4 illustrates the graph obtained in one of these simulations.

Figure 4

Graph for a $n_0 = 1x10\text{^}7$ with parameter variation

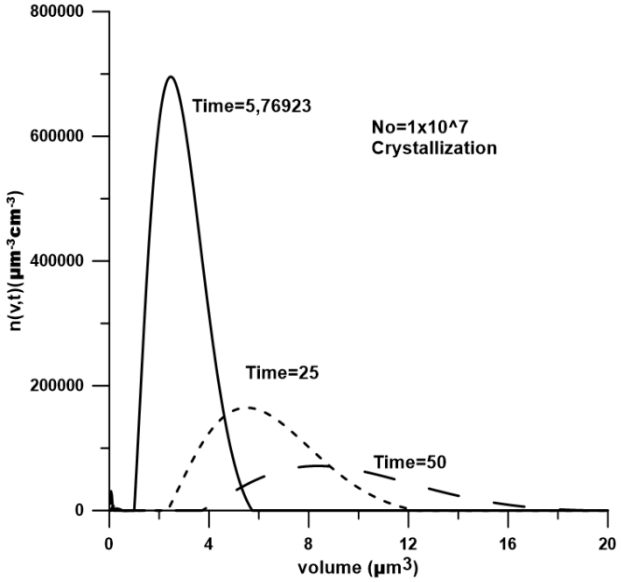

Source: Authors, 2025.

It can be seen that as time increases, the population density reduces even further, maintaining the expected behavior presented in the previous cases. Due to collisions and interactions between particles, even larger aggregates tend to emerge as time increases, a behavior illustrated in the graph, perceived by the reduction of small particles at times 25 and 50, concluding that most particles of size between 1 and 5 at time 5.76923 showed an increase in volume. Higher time values were tested in the code; however, as expected, the system tends to stabilize due to the reduction in population density and, consequently, in interactions between particles. Due to the nature of the process involving aerosols, which tend to occur in solute-poor environments, causing particle clusters to dissipate, it was not feasible to compare it at high time values.

In all four values of n_0, time and volume values smaller and larger than those presented in the graphs were tested to verify their influence on the behavior. In all cases, the population density tried to reach a minimum at the same rate as volume and time increased, since a longer time favors interactions between the particles in the system, resulting in a reduction in particle density. However, it is clear that the influence of time interferes more permanently in the system than the increase in volume, a factor clarified by the irrelevance of using excessively large values in the behavior of the curves. Furthermore, as n_0 increases, increasing volume values become relevant for analyses and simulations, since a larger population favors the emergence of larger particles.

5 CONCLUSION

In this present work, after analyzing the results obtained, it is concluded that the application of GITT to solve the PBE is valid, presenting results that are consistent with the literature and with the nature of the processes it represents. Furthermore, the robustness of the code created is highlighted, using the DIVPAG routine of the IMSL library in Fortran 90/95, covering a wide range of values, thus allowing complex and large-scale simulations.

The application of the established method demonstrated the ability of GITT to solve Integro-differential problems, facilitating the understanding of processes such as crystallization and aerosols, as well as phenomena related to colloidal chemistry and particulate systems. The application of the technique proved capable of providing an equation capable of describing the phenomena satisfactorily without the need for coarser approximations, a situation that was the objective of this present study.

The code produced generated graphs consistent with what was expected of these processes, characterized by the inversely proportional relationship between population density and particle size, and also having a coherent relationship with time, where the increase in time results in the emergence of larger particles due to contact between them in the medium. The code was stressed with numerous values of time, particle size and initial number of particles, proving capable of simulating processes with a wide scope for all these values, respecting those that are coherent.

REFERENCES

Alexopoulos, A. H., Roussos, A. I., & Kiparissides, C. (2024). Part I: Dynamic evolution of the particle size distribution in particulate processes undergoing combined particle growth and aggregation. Chemical Engineering Science, 59(22–23), 5751–5769. https://doi.org/10.1016/j.ces.2004.07.016

Batista, C. d. S. (2022). Solução de equações de balanço populacional usando a técnica da transformada de Laplace e filtro de partículas [Doctoral dissertation, Universidade Federal do Pará]. Repositório Institucional da UFPA.

Breit, F., Jakobsen, H. A., & von Harbou, E. (2025). Formulation of a mass-based population balance equation: Insights into derivation, mass transfer, and nondimensionalization. Chemical Engineering Communications, 212(7), 999–1012. https://doi.org/10.1080/00986445.2024.2311234

Costa, C. B. B., Maciel, M. R. W., & Filho, R. M. (2007). Considerations on the crystallization modeling: Population balance solution. Computers & Chemical Engineering, 31(7), 1832–1837. https://doi.org/10.1016/j.compchemeng.2006.11.005

Cotta, R. M., & Mikhailov, M. D. (1997). Integral transforms in computational heat and fluid flow. CRC Press.

Dantas, J., Silva, M., & Oliveira, P. (2002). Aplicação da transformada integral generalizada em equações de balanço populacional. Revista Brasileira de Engenharia Química, 19(3), 345–356.

Debnath, L., & Bhatta, D. (2007). Integral transforms and their applications (2nd ed.). Chapman & Hall/CRC.

Drake, R. L. (1972). A general mathematical survey of the coagulation equation. In G. M. Hidy & J. R. Brock (Eds.), Topics in current aerosol research: Part 2 (Vol. 3, pp. 201–276). Pergamon Press.

Falope, G. O., Jones, A. G., & Zauner, R. (2001). On modelling continuous agglomerative crystal precipitation via Monte Carlo simulation. Chemical Engineering Science, 56(7), 2567–2574. https://doi.org/10.1016/S0009-2509(00)00438-5

Gelbard, F., & Seinfeld, J. H. (1978). Numerical solution of the dynamic equation for particulate systems. Journal of Computational Physics, 28(3), 357–375. https://doi.org/10.1016/0021-9991(78)90060-9

Hulburt, H. M., & Katz, S. (1964). Some problems in particle technology: A statistical mechanical formulation. Chemical Engineering Science, 19(8), 555–574. https://doi.org/10.1016/0009-2509(64)85047-8

Jung, W. M., Kang, S. H., Kim, W. S., & Rhee, H. K. (2000). Particle morphology of calcium carbonate precipitated by gas-liquid reaction in a Couette-Taylor reactor. Chemical Engineering Science, 55(4), 733–747. https://doi.org/10.1016/S0009-2509(99)00395-6

Krutzer, L. L. M., van Diemen, A. J. G., & Stein, H. N. (1995). The influence of the type of flow on the orthokinetic coagulation rate. Journal of Colloid and Interface Science, 171(2), 429–438. https://doi.org/10.1006/jcis.1995.1200

Kufner, A. C., Rix, M., & Wohlgemuth, K. (2023). Modeling of continuous slug flow cooling crystallization towards pharmaceutical applications. Processes, 11(9), Article 2637. https://doi.org/10.3390/pr11092637

Lahiq, A. A., & Alshahrani, M. S. (2023). State-of-the-art review on various mathematical approaches towards solving population balanced equations in pharmaceutical crystallization process. Arabian Journal of Chemistry, 16(8), Article 104929. https://doi.org/10.1016/j.arabjc.2023.104929

Macêdo, E. N. (1999). A técnica da transformada integral aplicada em modelos de transporte de massa em meios porosos [Master's thesis, Universidade Federal do Pará]. Repositório Institucional da UFPA.

Miyagawa, H. K. (2014). A técnica da transformada integral generalizada no escoamento em dutos bidimensionais de geometria irregular na forma senoidal [Master's thesis, Universidade Federal do Pará]. Repositório Institucional da UFPA.

Ozisik, M. N., & Murray, R. L. (1974). On the solution of linear diffusion problems with variable boundary-condition parameters. Journal of Heat Transfer, 96(1), 48–51. https://doi.org/10.1115/1.3450131

Pagliolico, S., Marchisio, D., & Barresi, A. A. (1999). Influence of operating conditions on BaSO4 crystal size distribution and morphology in a continuous Couette-type precipitator. Journal of Thermal Analysis and Calorimetry, 56(3), 1423–1430. https://doi.org/10.1023/A:1010136721082

Panicker, A. S., Jabbour, R., & Mhaskar, P. (2023). Stochastic population balance methods for detailed modelling of flame-made aerosol particles. ResearchGate. https://doi.org/10.13140/RG.2.2.12345.67890

Pinar, Z. (2021). Studies on population balance equation involving aggregation and growth terms via symmetries. International Journal of Nonlinear Sciences and Numerical Simulation, 22(3–4), 437–446. https://doi.org/10.1515/ijnsns-2020-0123

Ramkrishna, D., & Borwanker, J. D. (1973). A puristic analysis of population balance I. Chemical Engineering Science, 28(6), 1423–1435. https://doi.org/10.1016/0009-2509(73)85005-0

Randolph, A. D. (1969). Effect of crystal breakage on crystal size distribution from a mixed suspension crystallizer. Industrial & Engineering Chemistry Fundamentals, 8(1), 58–69. https://doi.org/10.1021/i160029a011

Randolph, A. D., & Larson, M. A. (1988). Theory of particulate processes (2nd ed.). Academic Press.

Ramkrishna, D. (1985). The status of population balances. Reviews in Chemical Engineering, 3(1), 49–95. https://doi.org/10.1515/revce-1985-030104

Rigopoulos, S., & Jones, A. G. (2003). Finite element scheme for solution of the dynamic population balance equation. AIChE Journal, 49(5), 1277–1399. https://doi.org/10.1002/aic.690490519

Ruan, C., Dong, C., Liang, K., Liu, Z., & Bao, X. (2024). Euler's first-order explicit method–peridynamic differential operator for solving population balance equations of the crystallization process. CMES - Computer Modeling in Engineering & Sciences, 138(3), 3033–3049. https://doi.org/10.32604/cmes.2023.030607

Shweta, Hussain, S., & Kumar, R. (2024). Semi-analytical methods for population balance models involving aggregation and breakage processes: A comparative study. arXiv. https://doi.org/10.48550/arXiv.2403.11595

Singh, M., Kaur, G., & De Beer, T. (2020). Characterization of simultaneous evolution of size and composition distributions using generalized aggregation population balance equation. Pharmaceutics, 12(12), Article 1152. https://doi.org/10.3390/pharmaceutics12121152

Smoluchowski, M. von. (1917). Versuch einer mathematischen Theorie der Koagulationskinetik kolloider Lösungen. Zeitschrift für Physikalische Chemie, 92(2), 129–168. https://doi.org/10.1515/zpch-1917-9202

Sung, M. H., Choi, Y. S., & Kim, J. H. (2000). Agglomeration of yttrium oxalate particles produced by reaction precipitation in semi-batch reactor. Chemical Engineering Science, 55(11), 2173–2184. https://doi.org/10.1016/S0009-2509(99)00482-2

Tiong, S. I. X., Ahamed, F., & Ho, Y. K. (2025). Data-driven discovery of population balance equations for the particulate sciences. arXiv. https://doi.org/10.48550/arXiv.2502.09010

Verki, M. T., Halladj, R., Habidzadeh, S., & Shalmani, F. M. (2025). Crystallization and particle size distribution of hydrothermally synthesized SAPO-34: An experimental and population balance study. Scientific Reports, 15, Article 6301. https://doi.org/10.1038/s41598-025-56301-2

Zauner, R., & Jones, A. G. (2000). Determination of nucleation, growth, agglomeration, and disruption kinetics from experimental precipitation data: The calcium oxalate system. Chemical Engineering Science, 55(19), 4219–4232. https://doi.org/10.1016/S0009-2509(00)00098-3

Zhang, D., Li, Q., & Prigiobbe, V. (2022). Population balance modeling of homogeneous viral aggregation. Chemical Engineering Science, 247, Article 117035. https://doi.org/10.1016/j.ces.2021.117035